ACS Partner Journal
PRECISION CHEMISTRY
pubs.acs.org/PrecisionChem
Article

Quantum Computer Simulation of Molecules in Optical Cavity

Published as part of Precision Chemistry special issue "Quantum Landscape of Precision Chemistry".

Zirui Sheng,[#] Yufei Ge,[#] Jianpeng Chen, Weitang Li,[*] and Zhigang Shuai[*]

Cite This: *Precis. Chem.* 2025, 3, 326−336

ABSTRACT: Various phenomena have been observed in molecule−cavity coupled systems, which are believed to hold potential for applications in transistors, lasers, and computational units, among others. However, theoretical methods for simulating molecules in optical cavities still require further development due to the complex couplings between electrons, phonons, and photons within the cavity. In this study, motivated by recent advances in quantum algorithms and quantum computing hardware, we propose a quantum computing algorithm tailored for molecules in optical cavities. Our method, based on a variational quantum algorithm and variational boson encoders, has its effectiveness validated on both quantum simulators and hardware. For aggregates within the cavity, described by the Holstein−Tavis−Cummings model, our approach demonstrates clear advantages over other quantum and classical methods, as proved by numerical benchmarks. Additionally, we apply this method to study the H_2 molecule in a cavity using a superconducting quantum computer and the Pauli−Fierz model. To enhance accuracy, we incorporate error mitigation techniques, such as readout and reference-state error mitigation, resulting in an 86% reduction in the average error.

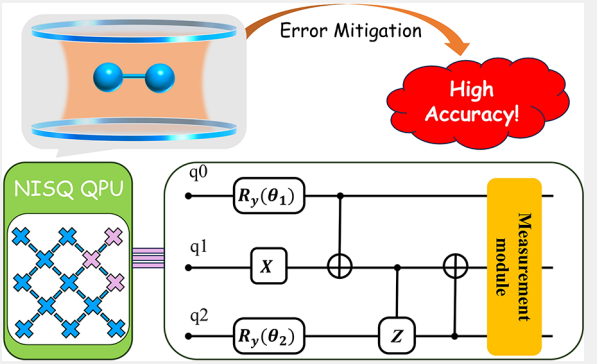

KEYWORDS: *optical cavity, polariton, quantum computing, quantum hardware simulation, error mitigation*

1. INTRODUCTION

Molecules can strongly interact with electromagnetic field in a small optical cavity, which forms quasi-particle named "polariton"[1] and brings novel physical phenomena.[2] The cavity systems have various potential applications including polariton lasing,[3,4] qubit for quantum computing,[5] polariton transistor,[6] controlling chemical dynamics,[7] and so on. Prosperity in cavity related experiments enhances the development of theories on polaritons and cavity systems further. The origin of the theoretical development is Tavis-Cummings (TC) model,[8,9] in which, cavity and molecules are simplified as two energy-level systems, while only taking into account the interactions between cavity and molecules. TC model introduces significant concepts of molecules in optical cavity such as "dark states", "lower polariton" and "upper polariton".[10] Meanwhile, the inherent simplifications in the TC model overlook several crucial features, such as the coupling between electron motion and molecular vibrations which plays a significant role in organic molecules; the intricate molecular structure, an important part in chemical processes; and the higher excitations of the cavity mode, which become significant under ultrastrong coupling conditions, among others. To address these issues, the Holstein−Tavis−Cummings (HTC) model[11,12] has been proposed to incorporate intermolecular exciton-vibration coupling. However, the HTC model is significantly more challenging to solve than the TC model due to the complexity of the exciton-vibration interactions. Considerable efforts have been made to tackle the HTC model, including methods such as treating nuclear motions classically,[13] applying *n*-particle approximations,[11] using mean-field approximations,[14] solving with the Lindblad master equation,[15] and employing tree tensor networks,[16] among others. Moreover, by expanding the HTC model, the effects of disorder[17] and intermolecular coupling[18] have also been explored. Additionally, the Pauli−Fierz (PF) Hamiltonian has been derived to facilitate ab initio calculations for molecules in cavities.[19] To solve the PF Hamiltonian, various approaches have been developed, including cavity quantum electrodynamics (QED) Hartree−Fock,[20] cavity QED density functional theory,[21,22] cavity QED configuration interaction,[20] cavity QED coupled cluster methods,[21,23] and diffusion quantum Monte Carlo.[24] Recently, first-principles-based dynamics of polaritons have also been established.[25]

Received: December 30, 2024
Revised: April 17, 2025
Accepted: April 18, 2025
Published: May 12, 2025

https://doi.org/10.1021/prechem.4c00108
Precis. Chem. 2025, 3, 326−336

To date, various Hamiltonians and methods have been proposed to address different aspects of the polaritonic system. However, current approaches face significant challenges in balancing computational accuracy with time efficiency, which impedes a deeper understanding of cavity systems. For instance, treating nuclear motions classically accelerates numerical simulations but overlooks quantum effects that are crucial in high-frequency vibrational modes. *n*-particle approximations speed up the simulation process by truncating the system to a finite number of phonons, but they may fail to accurately capture excited states. Tensor network methods provide an exact formal treatment of both photon/phonon and exciton dynamics, yet they require large bond dimensions to ensure numerical precision. In summary, the difficulty in theoretical simulations arises from the complex coupling between electrons, nuclear motions, and photons, as well as the vast number of states involved in light-matter interactions, leading to a challenging many-body problem.

The many-body problem in cavity systems with entanglement is fundamentally a quantum problem that is challenging to simulate efficiently on classical hardware. In contrast, the intrinsic properties of quantum hardware enable quantum computing to simulate quantum processes more efficiently, offering significant potential to overcome the limitations of classical methods. The concept of quantum computing stems from Feynman's insight that quantum systems can be used to simulate and solve quantum problems.[26] Since then, various quantum algorithms have been developed, including quantum Fourier transform,[27] phase estimation,[28] and Shor algorithm.[29] However, the practical application of these quantum algorithms remains constrained by the limitations of quantum hardware, particularly in the era of noisy intermediate-scale quantum (NISQ) devices.[30] To overcome these challenges, the variational quantum eigensolver (VQE) was proposed,[31,32] providing a promising approach for tackling problems in the NISQ era and demonstrating significant potential[33] which promoted a surge in the development of variational quantum algorithms (VQA).[34,35] In VQA, the quantum state is represented by a quantum circuit (i.e., ansatz) with a set of adjustable parameters, which can be optimized under specific conditions for particular targets (e.g., minimizing the ground-state energy). The diversity of ansatzes ensures the versatility of VQA. To date, VQA has been successfully applied to a wide range of problems, including quantum chemistry,[36−38] thermal properties of ground and excited states,[39,40] dynamical properties,[41,42] quantum approximate optimization,[43] and so on.

The intricate interactions between phonons, excitons, and polaritons can regulate the coherence of the system,[44,45] facilitate the formation of bound states in the continuum,[46] and modify the optical properties of materials.[47,48] However, due to the inherent challenges in dealing with bosons, there is still a lack of quantum algorithms for polariton chemistry that treat photons, phonons, and excitons/electrons equally. Some researchers have sought to enhance computational efficiency by introducing specialized schemes for mapping bosons onto qubits,[49] while others have focused on developing approximate optimization algorithms.[50] In one-hot encode, each $|m\rangle$ is encoded to $|00\cdots1_m\cdots00\rangle$, then the total number of qubits required scales as $O(N)$.[51,52] In binary encoding, each $|m\rangle$ is encoded to $\prod_i \left|\frac{m}{2^i}\right| \bmod 2\rangle$ represented by $O(\log N)$ qubits.[53,54] In terms of two-qubit gates required to simulate quantum operators such as $\hat{b}^\dagger \pm \hat{b}$ and $\hat{b}^\dagger \hat{b}$, one-hot encoding scales as $O(N)$ and binary encoding scales as $O(N \log N)$.[55] But this approach increases the depth of the quantum circuit. Recently, the development of variational boson encoder[56] (VBE) broadens the application of VQA further, which enable researchers to simulate the behavior of bosons more efficiently than one-hot encoding and binary encoding. Thus, we combine VQA with VBE to establish quantum algorithms for molecules in cavity.

Furthermore, one of the major challenges in realizing practical quantum computations for chemistry is the sensitivity of quantum devices to noise. Quantum devices are subject to various types and sources of noise, with the main categories including quantum decoherence, qubit flip noise, readout noise, and so on.[57] To mitigate or eliminate these noise effects in quantum computing, a range of solutions have been proposed. One approach focuses on correcting quantum errors internally within the quantum computer using techniques such as the introduction of logical qubits,[58,59] quantum feedback control,[60] and dynamical decoupling.[61] Another approach involves processing the results obtained from quantum computers to reduce errors, which has led to the development of various error mitigation methods. Several of these techniques have demonstrated improvements when computing the energies of small molecules using variational algorithms.[62,63] In our work, we adopt two error mitigation strategies to minimize errors: readout error mitigation (REM)[64] and reference-state error mitigation (RSEM).[65] REM corrects the intrinsic noise of the device using a response matrix, while RSEM further reduces errors by selecting a reference state.

The remainder of the paper is organized as follows. In Section 2, we introduce the model used to describe molecules in a cavity and present the framework of the VQA, where the photon/phonon basis is efficiently encoded using the VBE method. We also describe how to implement the quantum algorithm on a real quantum computer. In Section 3, we evaluate the accuracy of our method, comparing its performance with classical methods and other quantum algorithms that use different encoding schemes within the HTC model. Our approach demonstrates superior performance. Additionally, we calculate the potential energy curve of H_2 based on the PF model on quantum hardware, and apply two complementary error mitigation techniques.

2. METHODS

2.1. Theoretical Formula

The light-matter interaction Hamiltonian of molecules in a cavity is highly complex.[19] Researchers have primarily focused on two Hamiltonians that capture the key aspects of polariton chemistry: the HTC model[11] and the PF model.[20]

As shown in Figure 1(a), multiple (organic) molecules are placed within the cavity, which is modeled as a two-level system with a cavity mode frequency ω_c, exhibiting photon-like behavior. Each molecule is treated as a two-level exciton system with an excitation energy $\hbar\omega_0$. The molecules couple to the cavity mode with a coupling strength g_0. Additionally, intermolecular vibrations are considered, with each molecule coupled to several vibrational modes ω_m via coupling constants λ_m. The Hamiltonian of the HTC model is given below.

https://doi.org/10.1021/prechem.4c00108
Precis. Chem. 2025, 3, 326−336

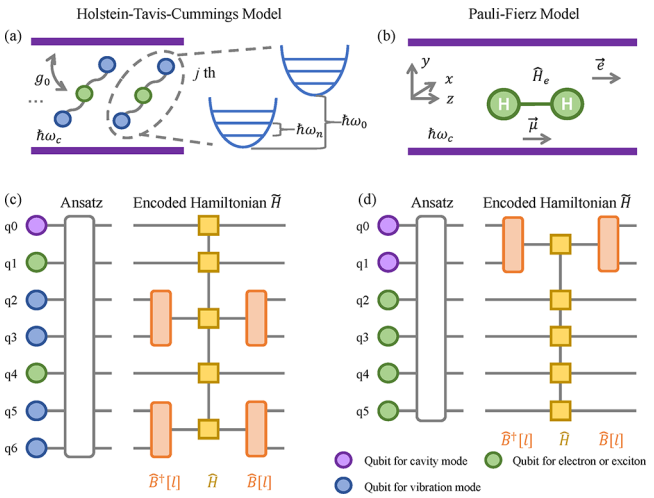

Figure 1. Graphic illustration of (a) the HTC model and (b) the PF model. Quantum circuits of (c) the HTC model, where one cavity mode (purple circle) is coupled to two excitons (green circles) and each exciton is coupled to one vibration mode, which is encoded by two qubits (blue circles), and (d) the PF model, where a hydrogen molecule (we need 4 qubits to represent the molecule when STO-3G basis and Jordan−Wigner transform are adopted, corresponding to green circles) is coupled to a cavity mode encoded by two qubits (purple circles). The orange rectangles corresponding to the encoding operators $\hat{B}^{\dagger}[l]$ and $\hat{B}[l]$. The yellow squares are the Hamiltonians before encoding.

$$\hat{H}_{\mathrm{HTC}} = \hbar\omega_c\hat{a}^{\dagger}\hat{a} + \hbar\omega_0\hat{\sigma}_j^{+}\hat{\sigma}_j^{-} + \sum_{j}^{N} g_0(\hat{a}^{\dagger}\hat{\sigma}_j^{-} + \hat{a}\hat{\sigma}_j^{+}) + \sum_{j}^{N}\sum_{m}^{M}\hbar\omega_m\hat{b}_{jm}^{\dagger}\hat{b}_{jm} + \sum_{j}^{N}\sum_{m}^{M}\hbar\lambda_m\omega_m\hat{\sigma}_j^{+}\hat{\sigma}_j^{-}(\hat{b}_{jm}^{\dagger} + \hat{b}_{jm}) \tag{1}$$

The first term represents the energy of the cavity, the second term corresponds to the energy of the excitons, the third term describes the coupling between the cavity and the excitons, the fourth term accounts for the vibrational energy, and the fifth term represents the exciton-vibration coupling. Here, j and m are indices for the molecules and vibrational modes, respectively. $\hat{a}^{\dagger}(\hat{a})$ and $\hat{b}_{jm}^{\dagger}(\hat{b}_{jm})$ are the creation (annihilation) operators for photons associated with the cavity mode and phonons corresponding to the molecular vibrational modes. N is the total number of molecules in the cavity, and M is the number of vibrational modes considered for each molecule. For simplicity, the zero-point energy of photons and phonons is neglected in the HTC model. Since the exciton satisfies intersite commutation and intrasite anticommutation relations, Pauli operator $\hat{\sigma}_j^{+}$ and $\hat{\sigma}_j^{-}$ are used as the creation and annihilation operators for the excitons.

The Pauli−Fierz (PF) model is commonly used for ab initio calculations of molecules in cavity.[20] As shown in Figure 1(b), a hydrogen molecule is placed in the cavity and couples to the cavity mode. In the PF model, the electronic structure of the molecule is treated in an ab initio manner. The PF model is described by the following Hamiltonian:

$$\hat{H}_{\mathrm{PF}} = \hat{H}_{\mathrm{M}} + \omega_c\left(\hat{a}^{\dagger}\hat{a} + \frac{1}{2}\right) - \sqrt{\frac{\omega_c}{2}}\lambda\hat{\mu}(\hat{a}^{\dagger} + \hat{a}) + \frac{1}{2}(\lambda\hat{\mu})^2 \tag{2}$$

The first term $\hat{H}_{\mathrm{M}}$ is the Hamiltonian of molecule, whose second quantization form is (following the convenience in quantum chemistry, atomic unit is adopted and $\hbar$, e are set as 1):

$$\hat{H}_{\mathrm{M}} = \sum_{pq} h_{pq}\hat{c}_p^{\dagger}\hat{c}_q + \frac{1}{2}\sum_{pqrs} h_{pqrs}\hat{c}_p^{\dagger}\hat{c}_q^{\dagger}\hat{c}_r\hat{c}_s + E_{\mathrm{nuc}} \tag{3}$$

h_{pq} and h_{pqrs} are one-electron and two-electron molecular orbital integrals:

$$h_{pq} = \int dr\chi_p^{*}(r)\left[-\frac{\nabla^2}{2} + U(r)\right]\chi_q(r) \tag{4}$$

$$h_{pqrs} = \int drdr'\chi_p^{*}(r)\chi_q^{*}(r')\frac{1}{|r-r'|}\chi_r(r')\chi_s(r) \tag{5}$$

Here, $\hat{c}_p^{\dagger}(\hat{c}_p)$ is creation (annihilation) operator of electron at orbital i. $\chi_p(r)$ is the spin orbital of electron, $-\frac{\nabla^2}{2}$ represents the kinetic energy of electrons, $U(r)$ corresponds to the Coulombic attractive energy between electrons and nucleus, $\frac{1}{|r-r'|}$ accounts for the Coulombic repulsive energy between electrons, and $E_{\mathrm{nuc}} = \sum_{AB}\frac{Z_AZ_B}{|R_A-R_B|}$ corresponds to the Coulombic repulsive energy between nucleus.

The second term represents the energy of the cavity with mode ω_c, which is treated as a photon. The third term describes the coupling between the cavity mode and the molecular dipole, while the fourth term accounts for the contribution of the molecular dipole. Here, $\hat{\mu} = \hat{\mu}_e + \hat{\mu}_N$ is the total dipole operator, which includes the electronic dipole $\hat{\mu}_e$ and nuclear dipole $\hat{\mu}_N$ (the latter can be treated as a constant μ_N when the molecular configuration is fixed). The coupling constant $\lambda = \sqrt{\frac{\hbar}{\epsilon_0 V}}\vec{e}$, where ϵ_0, V and $\vec{e}$ are the dielectric constant, the volume of the cavity, and the unit vector, respectively. Clearly, both $\hat{\mu}$ and λ are three-dimensional vectors corresponding to x, y, z direction. Since we focus only on diatomic molecules in our study, simplifications can be made. As shown in Figure 1(b), we align the molecular bond along the z-direction, such that $\hat{\mu}$ is parallel to the z-axis. By setting λ along the z-direction, the vectors $\hat{\mu}$ and λ can be simplified to $\hat{\mu}_z$ and λ_z, respectively. Consequently, the third and fourth terms can be expressed as

$$-\sqrt{\frac{\omega_c}{2}}\lambda\hat{\mu}(\hat{a}^{\dagger} + \hat{a}) = -\sqrt{\frac{\omega_c}{2}}(\lambda_z\hat{\mu}_{e,z})(\hat{a}^{\dagger} + \hat{a}) - \sqrt{\frac{\omega_c}{2}}\lambda_z\mu_N(\hat{a}^{\dagger} + \hat{a}) \tag{6}$$

$$\frac{1}{2}(\lambda\hat{\mu})^2 = \frac{1}{2}(\lambda_z\hat{\mu}_{e,z})^2 + \lambda_z\mu_{N,z}(\lambda_z\hat{\mu}_{e,z}) + \frac{1}{2}\lambda_z^2\mu_{N,z}^2 \tag{7}$$

Here, $\lambda_z\hat{\mu}_{e,z}$ and $(\lambda_z\hat{\mu}_{e,z})^2$ have the following second quantization formula:[20]

$$\lambda_z\hat{\mu}_{e,z} = \sum_{ij} d_{pq}\hat{c}_p^{\dagger}\hat{c}_q \tag{8}$$

$$(\lambda_z\hat{\mu}_{e,z})^2 = \sum_{pqrs} d_{pq}d_{rs}\hat{c}_p^{\dagger}\hat{c}_q^{\dagger}\hat{c}_r\hat{c}_s - \sum_{pqrs} D_{pq}\hat{c}_p^{\dagger}\hat{c}_q \tag{9}$$

Where

$$d_{pq} = -\lambda_z\int dr\chi_p^{*}(r)z\chi_q(r) \tag{10}$$

$$D_{pq} = -\lambda_z^2\int dr\chi_p^{*}(r)z^2\chi_q(r) \tag{11}$$

PySCF package[66] is adopted for obtaining related one-electron and two-electron integrals presented in eq 4, (5), (10) and (11). It should be mentioned that, the PF model arises from the dipole gauge transformation and the unitary phase transformation of the original light-matter interaction Hamiltonian under the Coulomb gauge.[20] Therefore, the photon number operator has the following form after transformation:[19]

$$\hat{N}_{\mathrm{ph}} = \hat{a}^{\dagger}\hat{a} - \sqrt{\frac{1}{2\omega_c}}\lambda\hat{\mu}(\hat{a}^{\dagger} + \hat{a}) + \frac{1}{2\omega_c}(\lambda\hat{\mu})^2 \tag{12}$$

For molecules in a cavity, researchers are primarily interested in the impact of light-matter coupling on the energies of the ground and excited states, as these are critical for chemical reactions and polariton lasing.

https://doi.org/10.1021/prechem.4c00108
Precis. Chem. 2025, 3, 326−336

It is worth mentioning that the systems studied in this work are highly simplified. In reality, optical cavities contain highly complex photonic modes and wavevectors. Thus, present classical methods face significant challenges, particularly in terms of memory and computational time while dealing with realistic molecular systems in optical cavities. Take the PF model as an example, if the system contains N_{mol} molecules collectively coupled to cavity modes N_{mode}, the Hilbert space dimension scales as $O(N_{el}^{N_{mol}} \times N_F^{N_{mode}})$ (according to $\hat{H}_{PF}$), where N_{el} is the number of electronic states and N_F is the Fock basis truncation. For instance, directly diagonalizing the polaritonic Hamiltonian results in memory requirements that scale exponentially with N_{mol} and N_{mode}. If $N_{el} = 2$, $N_F = 2$, $N_{mol} = 20$ and $N_{mode} = 2$, the simulation requires about 4.2×10^6 basis states, and the memory demand can exceed 100 GB even with sparse matrix techniques.[67] Mixed quantum-classical dynamics methods, such as surface hopping[68] and Ehrenfest dynamics,[69] also encounter severe computational overheads. These approaches require extensive sampling of trajectories to account for nonadiabatic effects, further increasing the computational complexity. In addition, for tensor network and other numerically exact methods, the truncation of the total Hilbert space must be carried out to perform meaningful theoretical explorations with realistic cavity designs and environments.[16,67] In contrast, the quantum algorithm leverages the unique properties of quantum superposition and entanglement to significantly reduce resource demands. For the simulation of the above large system, the formalism which will be introduced on Sec. 2.2 only requires 22 qubits. This demonstrates the superior scalability of quantum computing for simulating large cavity-coupled molecular systems.

2.2. Algorithm Realization on Quantum Simulator

As discussed in Section 2.1, polariton chemistry involves complex interactions between photons, phonons, and electrons/excitons. To map electron orbitals onto quantum qubits, the Jordan−Wigner transformation is used to convert intersite anticommuting Fermionic operators into Pauli operators:

$$\begin{cases} \hat{c}_j^\dagger = \prod_{k=1}^{j-1} (-\hat{\sigma}_k^z) \cdot \hat{\sigma}_j^+ \\ \hat{c}_j = \prod_{k=1}^{j-1} (-\hat{\sigma}_k^z) \cdot \hat{\sigma}_j^- \end{cases} \tag{13}$$

Furthermore, each photon or phonon requires 10−30 basis states for sufficient accuracy, making both one-hot encoding and binary encoding costly in terms of qubit usage or resulting in deep quantum circuits. To enhance the efficiency of the quantum algorithm, we map the photon/phonon basis to qubits using VBE.[56] VBE addresses the issue of the large number of bosonic basis states by recognizing that not all are necessary, and can instead be combined into a smaller set of essential basis states with adjustable variational parameters. This approach allows 10−30 original basis states to be effectively compressed into a few key combined bosonic states. Furthermore, these combined bosonic states can be encoded into qubit basis states via binary encoding, further reducing the qubit requirements.

Apart from the VBE part for bosons, our algorithm follows the framework of VQA. As shown in Figure 1(c) and (d), the electrons/excitons, cavity mode and vibration modes in HTC and PF model are mapped to several qubits. After setting the initial state $|\phi_0\rangle$ of qubits, an arbitrary state can be obtained via an ansatz with abundant tunable parameters.

Considering the conservation of the total excitation number $\hat{N} = \hat{a}^\dagger \hat{a} + \sum_j^N \hat{\sigma}_j^+ \hat{\sigma}_j^-$ as the quantum state evolves, along with the possibility for phonon creation and annihilation, the following ansatz is designed for the HTC model:

$$|\phi\rangle_{HTC} = \left\{ \prod_l^L \left[\prod_j^N \exp\theta_{lj}(\hat{a}^\dagger \hat{\sigma}_j^- - \hat{a}\hat{\sigma}_j^+) \prod_j^N \prod_m^M \exp\theta_{ljm} \hat{\sigma}_j^+ \hat{\sigma}_j^- (\hat{b}_{jm}^\dagger - \hat{b}_{jm}) \right] \right\} |\phi_0\rangle \tag{14}$$

Here, L is the number of ansatz layers, θ_{lj} and θ_{ljm} are adjustable parameters.

Motivated by the idea in variational Hamiltonian ansatz that all the terms in Hamiltonian (eq 2) that is not diagonal in the computational basis should exist in the ansatz, we devise the following ansatz for PF model:

$$|\phi\rangle_{PF} = \prod_l^L \left\{ \exp\left[\sum_{pq} i\theta_{lpq} \hat{c}_p^\dagger \hat{c}_q + \sum_{pqrs} i\theta_{lpqrs} \hat{c}_p^\dagger \hat{c}_q^\dagger \hat{c}_r \hat{c}_s + \sum_{pq} \theta'_{lpq} \hat{c}_p^\dagger \hat{c}_q (\hat{a}^\dagger - \hat{a}) + \sum_{pqrs} \theta'_{lpqrs} \hat{c}_p^\dagger \hat{c}_q^\dagger \hat{c}_r \hat{c}_s (\hat{a}^\dagger - \hat{a}) \right] \right\} |\phi_0\rangle \tag{15}$$

Here, L denotes the number of ansatz layers. The ansatz consists of terms related to (i) the movement of a single electron ($\hat{c}_p^\dagger \hat{c}_q$), (ii) scattering between two electrons ($\hat{c}_p^\dagger \hat{c}_q^\dagger \hat{c}_r \hat{c}_s$), (iii) the movement of a single electron with the creation/annihilation of a cavity photon ($\hat{c}_p^\dagger \hat{c}_q (\hat{a}^\dagger - \hat{a})$), and (iv) scattering between two electrons with the creation/annihilation of a cavity photon ($\hat{c}_p^\dagger \hat{c}_q^\dagger \hat{c}_r \hat{c}_s (\hat{a}^\dagger - \hat{a})$). Once the ansatz is defined for the system, the electron operators are transformed into Pauli operators using the Jordan−Wigner transformation and the encoding procedure for bosons, followed by conversion into the format suitable for a quantum circuit through Trotter decomposition. If only the ground state is of interest, the spin conservation relation can be applied to further simplify the form of the ansatz. Additionally, the terms $\hat{c}_p^\dagger \hat{c}_q$ and $\hat{c}_p^\dagger \hat{c}_q^\dagger \hat{c}_r \hat{c}_s$ in the ansatz ensure the conservation of electron number as the parameters $\{\theta\}$ are varied.

In addition to the classical VQA procedure, the Hamiltonian is further encoded through VBE in our work, as shown in Figure 1(c) and 1(d). In the HTC model, each cavity mode is coupled to 2 excitons, and each exciton is coupled to a single vibration mode, which is encoded by two qubits, resulting in a total of 7 qubits. In the PF model, the hydrogen molecule is coupled to a cavity mode encoded by 2 qubits. Here, 4 qubits are required to represent the molecule when using the STO-3G basis and Jordan−Wigner transformation, leading to a total of 6 qubits. Notably, when conducting experiments on quantum hardware, we further apply the parity transformation to conserve qubits. This approach will be detailed in the following section. When employing different encoding schemes for bosons, the depth of the circuit is influenced by the correspondence relationship of bosons and qubits. We will provide a detailed analysis of this relationship in Sec. 3.1. The encoded Hamiltonian is given by the following formula:

$$\tilde{H} = \prod_l \hat{B}[l] \hat{H} \prod_l \hat{B}^\dagger[l] \tag{16}$$

Here, l is the index of cavity mode or vibrational mode that need encoding. $\hat{B}[l]$ is the encoding operator $\hat{B}[l] = B[l]_{nm}|n\rangle\langle m|$, where $B[l]$ denotes the encoding matrix, $|n\rangle$ is the encoded qubit basis, and $\langle m|$ is the basis of cavity/vibration mode. The size of matrix $B[l]$ is $2^{N_Q} \times d$, where N_Q represents the number of qubits spent for each mode and d is the number of bases adopted in each mode. $\hat{B}[l]$ satisfies orthonormal constraint $\hat{B}[l]\ \hat{B}^\dagger\ [l] = \hat{I}$. If $2^{N_Q} = d$, $\hat{B}[l]$ will be equal to the identity operator in the whole optimization procedure, corresponding to the case that the bosons are directly encoded by binary encoding. The energy E of the system can be calculated by

$$E = \langle\phi|\tilde{H}|\phi\rangle \tag{17}$$

In algorithms both $\{\theta_j\}$ and $\{B[l]\}$ can be adjusted to reach the lowest ground state energy, and the parameters $\{\theta_j\}$ can be updated as below:

https://doi.org/10.1021/prechem.4c00108
Precis. Chem. 2025, 3, 326−336

$$\frac{\partial\langle\phi|\tilde{H}|\phi\rangle}{\partial\theta_j} = 0 \tag{18}$$

The matrix $B[l]$ can be updated by solving the following equation:

$$(1 - \hat{P}[l])\langle\phi|\tilde{H}'[l]|\phi\rangle = 0 \tag{19}$$

Where

$$\hat{P}[l] = \hat{B}^{\dagger}[l]\hat{B}[l] \tag{20}$$

And

$$\tilde{H}'[l] = \prod_{k\neq l}\hat{B}[k]\hat{H}\prod_{k}\hat{B}^{\dagger}[k] \tag{21}$$

By updating $\{\theta_j\}$ and $\{B[l]\}$ sequentially, we can obtain the ground state. If we want to calculate Kth excited states, we can use the knowledge of zeroth (ground state), first, ..., (K - 1)th excited states to modify the form of Hamiltonian in eq 1 or eq 2 to[70]

$$\hat{H} = \hat{H}_{\mathrm{HTC(PF)}} + \prod_{k=0}^{K-1}\alpha_k|\phi_k\rangle\langle\phi_k| \tag{22}$$

Here, k is the index of state, a_k is set as 20 in our simulation. Note that a_k needs careful test to balance the strength of orthogonal condition and the difference between the energy levels.

In summary, the quantum algorithm for calculating ground state and low-energy excited states of cavity systems is presented below as Algorithm 1. The simulations are carried out on TenCirChem[71] and TensorCircuit.[72]

Algorithm 1

Input: parameters presented in HTC model (Eq.(1)) or PF model (Eq.(2)), number of excited states K that needs calculation. Initiate previous state vector set as {}.
For $n = 0, 1, 2, \ldots, K$:
    Generate quantum circuits, initialize $\{\theta\}$ and $\{B[l]\}$, and generate Hamiltonian through input and previous state vector set. Calculate energy E through Eq. (17)
    While True:
        Update $\{\theta\}$ through Eq. (18)
        Update $\{B[l]\}$ through Eq. (19)
        Calculate energy E' through Eq. (17)
        If $|E - E'| <$ threshold:
            break
        $E = E'$
    Add state $|\phi\rangle$ state vector set, and the kth excited state energy is E_k
Output: ground and excited state energy $\{E_0, E_1, \ldots, E_K\}$

2.3. Running on Quantum Hardware

We will test the behavior of H_2's PF model on real quantum computer. To save the number of qubits further, we adopt parity transformation,[73] utilizing electron and spin conservation. As shown in Figure 2, parity transform and Jordan–Wigner transform have the same behavior and saves two qubits when the spin number and electron number are fixed. The updating procedure of $\{\theta\}$ is down through the VQE on classical computer, only measurements are down on quantum computer. The whole steps still follow Algorithm 1, while the only difference is that on step 3 we get the energy from 4096 measurements for each set of parameters.

Besides, $\{B[l]\}$ are obtained via solving eq 19. To realize the target, the key step is to express

$$\hat{G}[l] = \phi|\tilde{H}'[l]|\phi\rangle \tag{23}$$

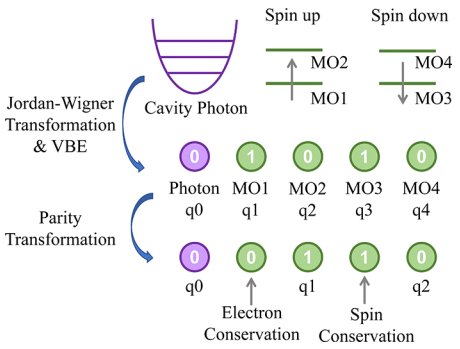

Figure 2. Graphic illustration of the Jordan–Wigner transform and parity transform in encoding molecular orbitals (MO). Here, we take the initial guess of H_2 molecule in the cavity as an example (the direct product of the Hartree–Fock state of H_2 and the ground state of the isolated photon).

as a function of $B[l]$. For simplicity, we suppose the Hamiltonian can be expressed as a sum of product

$$\hat{H} = \sum_{a}^{M}\hat{h}_a = \sum_{a}^{M}\prod_{k}\hat{h}[k]_a \tag{24}$$

Here, $\hat{h}[k]_a$ is the operator of kth basis in $\hat{h}_a$, a is the index of Hamiltonian terms, and k is the index of qubit. Note that $G[l]$ is a matrix with size $2^{N_Q} \times d$. The matrix element $G[l]_{mn}$ of $G[l]$ is defined as

$$G[l]_{mn} = \langle\phi|n\rangle m|\tilde{H}'[l]|\phi\rangle \tag{25}$$

Here, $|n\rangle$ and $|m\rangle$ are the basis of 2^{N_Q} qubit state and d boson state corresponding to the lth encoder. $G[l]_{mn}$ can be calculated via following equation:

$$[l]_{mn} = \sum_{a}^{M}\sum_{m'n'}h[l]_{amm'}B[l]_{m'n'}J[l]_{ann'} \tag{26}$$

Where

$$[l]_{ann'} = \langle\phi|n\rangle\left\langle n'\left|\prod_{k\neq l}\tilde{h}[k]_a\right|\phi\right\rangle \tag{27}$$

$J[l]_{\mathrm{ann}'}$ can be calculated on quantum computer, where $\hat{h}[k]_a = \hat{B}[k]\hat{h}[k]_a\hat{B}^{\dagger}[k]$, and both $\hat{h}[k]_a$ and $|n\rangle\langle n'|$ can be transformed to Pauli strings. ($|n\rangle\langle n'|$ is not Hermitian while it can be viewed as the linear combination of two Hermitian parts: $|n\rangle\langle n'| + |n'\rangle\langle n|$ and $\mathrm{i}(|n\rangle\langle n'| - n'\rangle\langle n|)$).

We employed the hardware-efficient ansatz[74] (HEA) for experiments on real quantum hardware. While the VHA is usually designed according to the physical symmetries of the Hamiltonian, it typically requires a smaller parameter space and achieves superior accuracy and faster convergence than HEA in numerical simulations. However, VHA becomes less practical for complex systems involving multiqubit couplings. Such scenarios often demand deep circuits with a large number of noise-sensitive two-qubit gates. In contrast, the HEA features a shallow circuit architecture, primarily composed of single-qubit gates and local entanglement, making it more resilient to hardware noise. Despite its scalability in principle, the HEA suffers from the barren plateau problem, where gradient magnitudes decay exponentially with system size, posing significant challenges for optimization. Considering these trade-offs, we utilized the VHA in numerical simulations to capitalize on its precision and efficiency, while opting for the HEA in hardware experiments to accommodate the constraints of NISQ devices.

https://doi.org/10.1021/prechem.4c00108
Precis. Chem. 2025, 3, 326–336

Table 1. Energy of HTC Hamiltonian under Different Computational Parameters[a]

Index of Data	L	N_Q	d	$E_0 - E_{0,\mathrm{ref}}$ (meV)	$E_1 - E_{1,\mathrm{ref}}$ (meV)	$E_2 - E_{2,\mathrm{ref}}$ (meV)	$E_3 - E_{3,\mathrm{ref}}$ (meV)
0 (Without VBE)	9	2	4	8.623	43.632	30.424	102.510
1	3	1	8	2.785	39.956	−10.659	67.721
2	3	1	16	2.719	40.578	−4.256	85.547
3	3	2	16	0.202	0.736	4.015	18.417
4	6	2	16	0.094	0.213	0.290	0.135
5	9	2	16	0.012	0.136	0.034	0.137

[a]Here $N = 2$, $\lambda_m = 2$, $\hbar\omega_m = 0.2$ eV, $\hbar\omega_c = \hbar\omega_0 = 1.0$ eV, and $g_0 = 1.0$ eV. L is the number of ansatz layers, N_Q is the number of qubits spent for each mode, and d is the number of basis adopted in each mode. E_0, E_1, E_2, and E_3 correspond to the energy of ground state, first excited state, second excited state and third excited state. The energy $E_{i,\mathrm{ref}}$ for the reference is calculate via exact diagonalization under $d = 16$, and $E_0 - E_{0,\mathrm{ref}}$ measures the error of calculated energy. Note that the chemical accuracy is about 43.5 meV.

Table 2. Energy of PF Hamiltonian under Different Computational Parameters[a]

Index of Data	L	N_Q	d	$E_0 - E_{0,\mathrm{ref}}$ (meV)	$E_1 - E_{1,\mathrm{ref}}$ (meV)	$E_2 - E_{2,\mathrm{ref}}$ (meV)	$E_3 - E_{3,\mathrm{ref}}$ (meV)
0 (Without VBE)	6	2	4	45.634	657.727	3409.534	4.980
1	3	1	8	257.121	669.781	7819.386	13610.680
2	3	1	16	257.121	669.618	7819.386	13610.680
3	3	2	16	$<10^{-3}$	0.136	0.003	4.980
4	9	2	16	$<10^{-3}$	0.136	0.027	4.980

[a]Here, the H_2 molecule is adopted, with H−H bond length set as $R(\mathrm{H-H}) = 0.053$ nm, cavity mode $\hbar\omega_c = 13.6$ eV, and $\lambda = 1.0$. L is the number of ansatz layers, N_Q is the number of qubits for each mode, and d is the number of basis adopted in each mode. E_0, E_1, E_2, and E_3 correspond to the energy of ground state, first excited state, second excited state and third excited state. The energy $E_{i,\mathrm{ref}}$ for the reference is calculated via exact diagonalization under $d = 32$, and $E_0 - E_{0,\mathrm{ref}}$ measures the error of calculated energy. Note that the chemical accuracy is about 43.5 meV.

3. RESULTS AND DISCUSSION

3.1. The Accuracy of the Quantum Algorithm

First, we evaluate the accuracy of our algorithm. As shown in Table 1, we calculate the ground state and low-energy excited state energies in the HTC model under different conditions. The data obtained from exact diagonalization is used as the reference. The depth of the quantum circuit increases rapidly as the number of qubits per boson increases in binary encoding, making it difficult to achieve for large numbers of qubits. Therefore, an upper limit of 2 qubits per boson is set in our work. As seen in "Data 0" in Table 1, when the VBE is not used, the errors in the reference energies $E_i - E_{i,\mathrm{ref}}$ are significantly larger compared to the cases where VBE is applied. Additionally, the errors in the higher excitation energies ($E_1 - E_{1,\mathrm{ref}}$, $E_2 - E_{2,\mathrm{ref}}$, $E_3 - E_{3,\mathrm{ref}}$) are considerably larger than the error in the ground state energy ($E_0 - E_{0,\mathrm{ref}}$). Moreover, considering that chemical accuracy is approximately 43.5 meV, the calculated energies of the excited states are unreliable. By comparing "Data 0" with other data sets, we suggest that the large errors in the calculated energies for "Data 0"" primarily arise from the lack of vibrational basis states. As shown in Table 1, as the number of basis states increases, the accuracy of the calculated energies improves significantly. Even the case with $N_Q = 1$ and VBE ("Data 1" and "Data 2") shows better performance than the case with $N_Q = 2$ without VBE ("Data 0"). Additionally, we should note the following: (i) the number of encoded bosonic basis states should not be too small; $N_Q = 1$ is insufficient for accurately calculating excited state energies (see "Data 1" and "Data 2"), indicating strong entanglement between phonons and excitons; (ii) six layers of ansatz are required, and further increases in the number of ansatz layers do not significantly improve the results (see "Data 4" and "Data 5").

Next, we test the performance of our algorithm using the PF Hamiltonian, as shown in Table 2. Similar to the results in Table 1, we observe a significant improvement in accuracy when VBE is applied, as seen by comparing "Data 0" and "Data 3". However, unlike the case in the HTC model, the $N_Q = 1$ case with VBE ("Data 1" and "Data 2") performs much worse than the case without VBE, particularly in calculating excited state energies. This behavior arises from the strong entanglement between electron orbitals and cavity modes, making it challenging for two encoded modes to be explicitly represented in the optimization process. Once an adequate number of encoded basis states is used, increasing d leads to a systematic reduction in errors. Additionally, we find that $L = 3$ is sufficient for achieving a converged result.

In summary, we find in Tables 1 and 2 that as long as the number of qubits for each mode N_Q is enough, increasing the number of basis of boson mode via VBE increases the accuracy systematically. We further evaluate the accuracy and efficiency of our method across different strengths of exciton-cavity coupling g_0, exciton−phonon coupling λ and cavity energy $\hbar\omega_c$. The n-particle approximation refers to considering only states with no more than n phonons in the calculation. Here, we use one-particle and two-particle approximations for comparison. As shown in Figure 3, we find that (i) when the number of encoded qubits per boson mode is fixed at 2, the numerical errors for different methods follow this order: VQA with VBE < VQA with binary encoding < two-particle approximation < VQA with one-hot encoding < one-particle approximation. (ii) As g_0 decreases, or λ, $\hbar\omega_c$ increases, the electron−phonon coupling becomes more significant, and the numerical errors for all methods increase rapidly, except for our algorithm. (iii) The numerical errors of VQA with VBE across all conditions are well below the chemical accuracy threshold, demonstrating the robustness and validity of our algorithm over the entire parameter space.

3.2. Experiments on a Quantum Computer

Finally, we test our algorithm on quantum hardware following methods presented in Sec. 2.3. We utilize the Tianji S2 chip from Tencent Quantum Cloud Lab, which features 13 qubits

https://doi.org/10.1021/prechem.4c00108
Precis. Chem. 2025, 3, 326−336

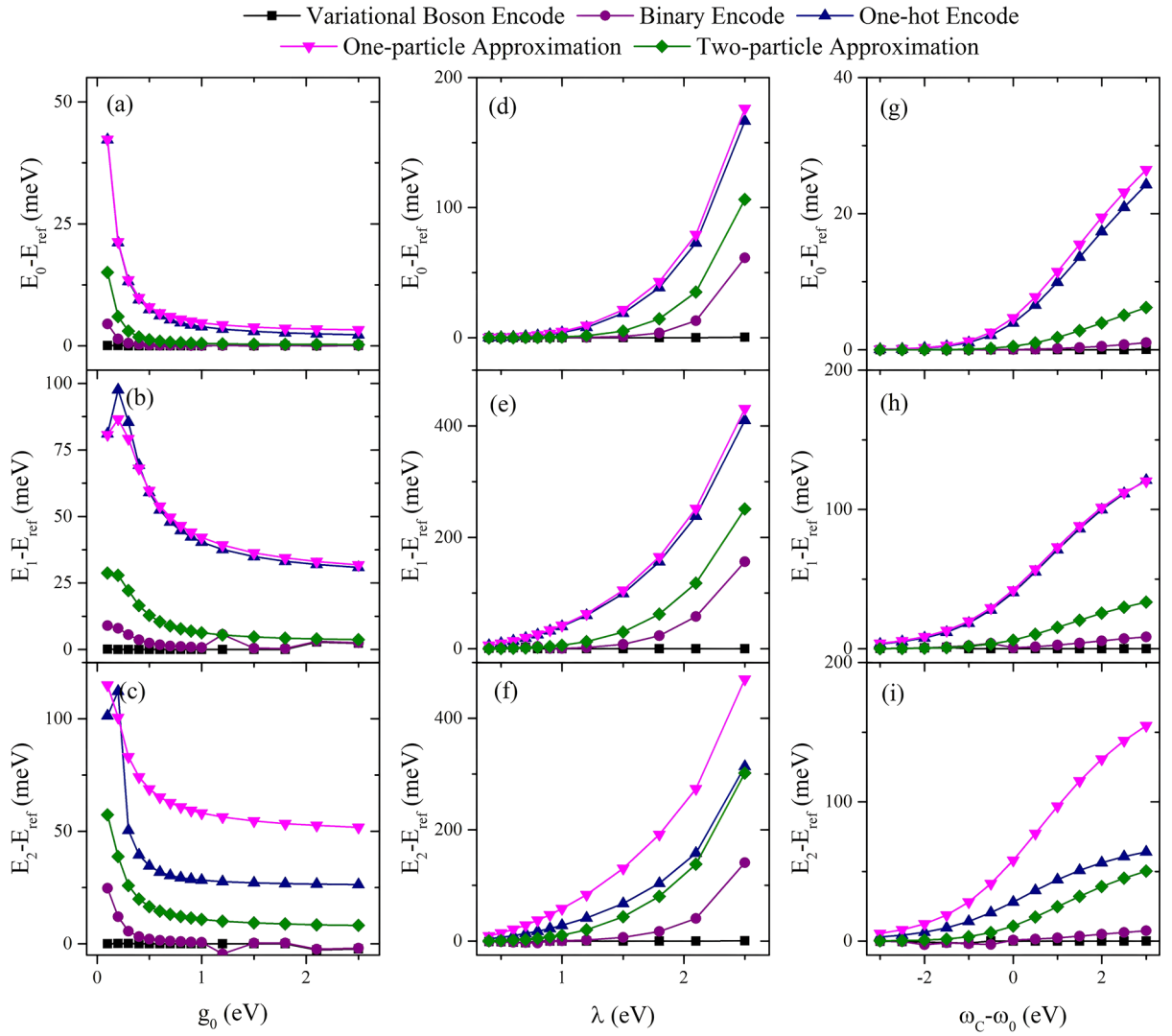

Figure 3. Numerical errors of different methods at (a–c) different strengths of exciton–cavity coupling g_0, (d–f) different strengths of exciton–phonon coupling λ, and (g–i) different cavity energies $\hbar\omega_c$. $\lambda_m = 1$, $\hbar\omega_c = 0.2$ eV, $\hbar\omega_c = \hbar\omega_0 = 1.0$ eV, and $g_0 = 1.0$ eV when these parameters are not independent variables. $L = 2$, $N = 2$, $N_Q = 2$, and $d = 16$ are set in numerical calculations. The reference energy is calculated via exact diagonalization.

interconnected via an adjustable coupler. The details of this chip can be found in Table 3. To decrease the depth of quantum circuit, the HEA presented in Figure 4(a) is applied, we employed 3 qubits. As illustrated in Figure 2, the photon state was encoded on qubit q0, while the electronic states were encoded on qubits q1 and q2. In constructing the ansatz, we implemented two rotating gates with adjustable parameters. The first R_y gate was applied to q0 to regulate the photon state, while the second R_y gate was applied to q2, which was combined with two two-qubit gates between q1 and 2 and an X gate on q1 to manipulate the electronic state. The coupling between the photon and electronic states was realized through a CNOT gate acting on qubits q0 and q1.

Table 3. Fundamental Parameters of Tencent Tianji S2 chip

Parameter	Average Value
Longitudinal Coherence Time	102.9 μs
Transverse Coherence Time	11.9 μs
Single-Qubit Gate Fidelity	99.94%
Two-Qubit Gate Fidelity	99.33%
Readout Fidelity	F0: 97.22%
	F1: 94.73%

To improve the accuracy of the measurement results obtained from noisy quantum devices, error mitigation schemes are indispensable. There are several valuable methods for mitigating noise in quantum computing, including zero-noise extrapolation (ZNE) and probabilistic error cancellation (PEC), among others. ZNE involves running the quantum circuit at multiple noise levels by artificially increasing the noise through techniques such as inserting additional gates or extending gate durations. However, the accuracy of ZNE heavily depends on the choice of extrapolation model. Given the complex noise characteristics of NISQ hardware, which are often poorly captured by simple extrapolation models (e.g., linear or polynomial), the results may lack reliability. Furthermore, ZNE is primarily effective for mitigating gate operation noise. Since the circuit is subject to many kinds of noise, the potential impact of ZNE may be limited. PEC theoretically allows for the complete cancellation of noise by constructing inverse operations based on a precise noise

https://doi.org/10.1021/prechem.4c00108
Precis. Chem. 2025, 3, 326–336

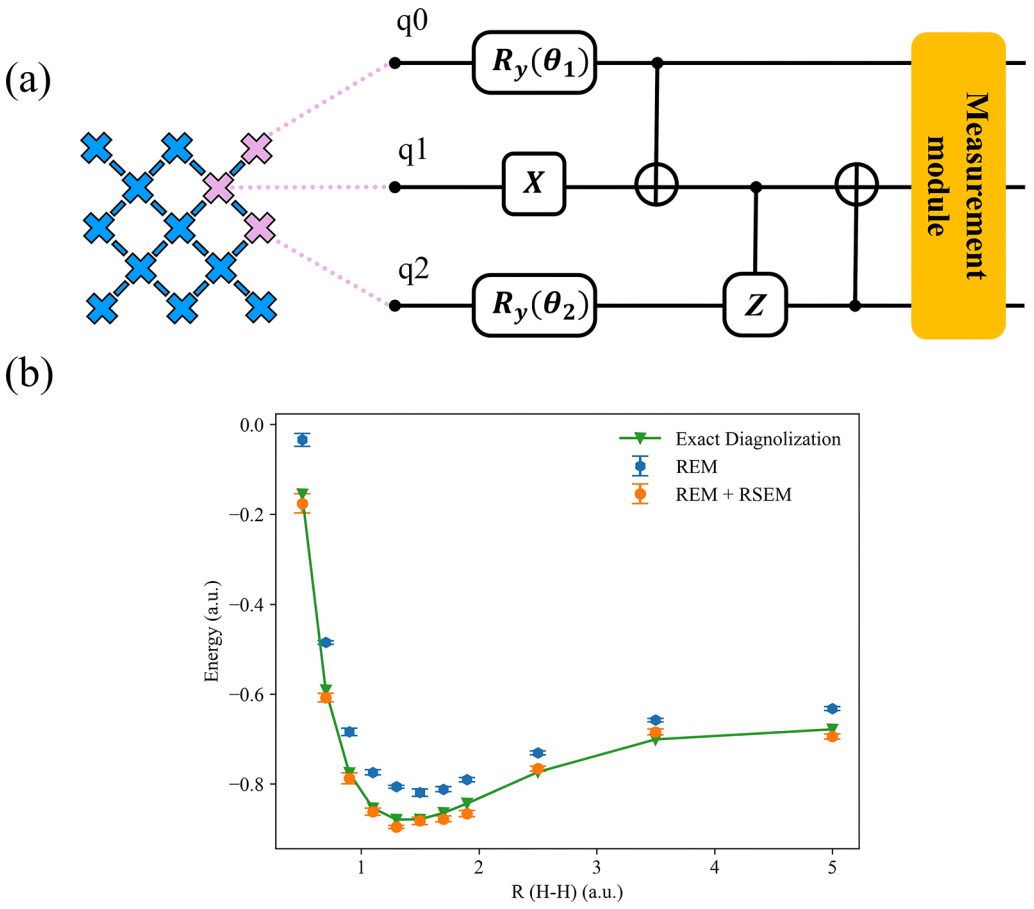

Figure 4. (a) The HEA designed for quantum hardware experiments. Three qubits out of 13 qubits of a superconducting quantum processor and a two-parameter circuit are used for simulation. (b) The calculated potential energy curve of H_2 molecule in cavity on quantum hardware after REM (orange rounds) or after both REM and RSEM (blue hexagons). The curve calculated via exact diagonalization is also presented as benchmark (green triangles).

model. However, this method requires exceptionally accurate noise characterization, which is challenging to achieve on NISQ devices with highly dynamic noise profiles. Moreover, PEC significantly increases the computational cost due to the need for repeated sampling and the execution of additional corrective operations. Given these considerations, we opted for simpler and more hardware-compatible error mitigation techniques, namely REM[64] and RSEM.[65]

An ideal quantum measurement in the computational basis can be expressed in terms of a positive operator-valued measurement, and if all the elements have no nontrivial off-diagonal terms, the measurement noise channel can be treated as a classical noise channel. In this case, the transformation between the ideal and noisy measurement probability distributions can be described using a response matrix $\mathbf{\Lambda}$: $\mathbf{p}_{\text{ideal}} = \Lambda^{-1}\mathbf{p}_{\text{noisy}}$, $\mathbf{p}_{\text{noisy}}$ and $\mathbf{p}_{\text{noisy}}$ represent the ideal and noisy probability distributions. If we assume the noise acts independently on each qubit, then the response matrix can be written as $\Lambda = \prod_{i=1}^{N_q} \begin{pmatrix} 1-p_i & q_i \\ p_i & 1-q_i \end{pmatrix}$. Then by acting Λ^{-1} on $\mathbf{p}_{\text{noisy}}$, we can accomplish the REM scheme. And to further improve the accuracy, we apply RSEM, which can be applied alongside existing mitigation procedures. The RSEM method relies on the selection of a reference state, with the Hartree–Fock state chosen here, as it provides a computationally efficient mean-field description of the electronic potential. After preparing the parametrized reference state $|\Psi(\vec{\theta}_{ref})\rangle$, the resulting energy error ΔE_{RSEM} at the reference parameters $\vec{\theta}_{ref}$ is $\Delta E_{RSEM} = E_{VQE}(\vec{\theta}_{ref}) - E_{exact}(\vec{\theta}_{ref})E_{exact}(\vec{\theta}_{ref})$. Here $E_{exact}(\vec{\theta}_{ref})$ is the noiseless solution evaluated on classical computer, and $E_{VQE}(\vec{\theta}_{ref})$ refers to the energy evaluated from measurements on a quantum computer. We note that $\vec{\theta}_{ref}$ is chosen such that a classical solution to the problem is feasible. By subtracting the error ΔE_{RSEM} when performing formal energy calculations, the results obtained from the quantum computer can be further promoted.

We then conduct quantum hardware experiments. To get the potential energy curve of H_2 molecule in cavity, we use the Hamiltonian of PF model with setting $\lambda = 1$ and $\omega_c = 0.5$. Eleven discrete interatomic distances are selected for calculation, and for each interatomic distance we perform four sequential hardware experiments. In the VBE approach, the number of basis states adopted for each mode is set to $d = 8$. All data points and error bars in Figure 4(b) are derived from the average and standard deviation of these experiments. After applying the REM scheme, our algorithm accurately captures the general trend of the H_2 potential energy surface on the quantum hardware. The average error across all data points, relative to the exact solution, is approximately 0.07 hartree. Subsequently, when both the REM and RSEM schemes are applied, our algorithm yield improved results across the entire potential energy curve, with the average error reduced to a small value of about 9.6 mH relative to the exact

https://doi.org/10.1021/prechem.4c00108
Precis. Chem. 2025, 3, 326−336

solution. This average error has a reduction of 86% compared to the results obtained by REM alone. Such precise results demonstrate the feasibility of our algorithm after incorporating both error mitigation techniques.

4. CONCLUSIONS

In summary, we have developed a quantum algorithm for molecules in a cavity, described by either the HTC or PF model. We advance the VBE approach by addressing systems with complex electron−phonon-photon couplings and diverse boson types, while pioneering the computation of low-energy excited states. Furthermore, we conducted experiments on a real quantum computer based on the PF model Hamiltonian. By applying two error mitigation techniques, we obtained results that closely align with the classical exact solution, showing the critical role of selecting appropriate error mitigation strategies to improve computational accuracy in the current NISQ era. Hindered by the noise on NISQ hardware, the systems studied in this work have limited size. Although this work is just the starting point, it highlights the potential of quantum algorithms in tackling complex systems like cavity-based molecule interactions. As quantum hardware and algorithm continue to advance, we believe our approach will provide valuable insights into cavity systems, paving the way for further theoretical and practical breakthroughs.

AUTHOR INFORMATION

Corresponding Authors

Weitang Li − *School of Science and Engineering, The Chinese University of Hong Kong, Shenzhen, Guangdong 518172, China;* orcid.org/0000-0002-8739-641X; Email: liwt31@gmail.com

Zhigang Shuai − *School of Science and Engineering, The Chinese University of Hong Kong, Shenzhen, Guangdong 518172, China;* orcid.org/0000-0003-3867-2331; Email: shuaizhigang@cuhk.edu.cn

Authors

Zirui Sheng − *School of Science and Engineering, The Chinese University of Hong Kong, Shenzhen, Guangdong 518172, China*

Yufei Ge − *Department of Chemistry, MOE Key Laboratory for Organic OptoElectronics and Molecular Engineering, Tsinghua University, Beijing 100084, China*

Jianpeng Chen − *School of Science and Engineering, The Chinese University of Hong Kong, Shenzhen, Guangdong 518172, China*

Complete contact information is available at: https://pubs.acs.org/10.1021/prechem.4c00108

Author Contributions

#Z.S. and Y.G. contributed equally

Notes

The authors declare no competing financial interest.

ACKNOWLEDGMENTS

This work is supported by the National Natural Science Foundation of China (Grant Nos. T2350009 and 22433007), Guangdong Provincial Natural Science Foundation (Grant No. 2024A1515011185), the Shenzhen City "Pengcheng Peacock" Talent Program, and Shenzhen Science and Technology Program (No. KQTD20240729102028011). W.L. is supported by the Young Elite Scientists Sponsorship Program by CAST (2023QNRC001) and University Development Fund (UDF01003789).

REFERENCES

(1) Herrera, F.; Spano, F. C. Theory of Nanoscale Organic Cavities: The Essential Role of Vibration-Photon Dressed States. *ACS Photonics* **2018**, *5* (1), 65−79.

(2) Daskalakis, K. S.; Maier, S. A.; Murray, R.; Kéna-Cohen, S. Nonlinear Interactions in an Organic Polariton Condensate. *Nat. Mater.* **2014**, *13* (3), 271−278.

(3) Arnardottir, K. B.; Moilanen, A. J.; Strashko, A.; Törmä, P.; Keeling, J. Multimode Organic Polariton Lasing. *Phys. Rev. Lett.* **2020**, *125* (23), 233603.

(4) Kéna-Cohen, S.; Forrest, S. R. Room-Temperature Polariton Lasing in an Organic Single-Crystal Microcavity. *Nat. Photonics* **2010**, *4* (6), 371−375.

(5) Demirchyan, S. S.; Chestnov, I. Yu.; Alodjants, A. P.; Glazov, M. M.; Kavokin, A. V. Qubits Based on Polariton Rabi Oscillators. *Phys. Rev. Lett.* **2014**, *112* (19), 196403.

(6) Zasedatelev, A. V.; Baranikov, A. V.; Urbonas, D.; Scafirimuto, F.; Scherf, U.; Stöferle, T.; Mahrt, R. F.; Lagoudakis, P. G. A Room-Temperature Organic Polariton Transistor. *Nat. Photonics* **2019**, *13* (6), 378−383.

(7) Herrera, F.; Spano, F. C. Cavity-Controlled Chemistry in Molecular Ensembles. *Phys. Rev. Lett.* **2016**, *116* (23), 238301.

(8) Tavis, M.; Cummings, F. W. Exact Solution for an N -Molecule—Radiation-Field Hamiltonian. *Phys. Rev.* **1968**, *170* (2), 379−384.

(9) Tavis, M.; Cummings, F. W. Approximate Solutions for an N -Molecule-Radiation-Field Hamiltonian. *Phys. Rev.* **1969**, *188* (2), 692−695.

(10) Ribeiro, R. F.; Martínez-Martínez, L. A.; Du, M.; Campos-Gonzalez-Angulo, J.; Yuen-Zhou, J. Polariton Chemistry: Controlling Molecular Dynamics with Optical Cavities. *Chem. Sci.* **2018**, *9* (30), 6325−6339.

(11) Spano, F. C. Exciton-Phonon Polaritons in Organic Microcavities: Testing a Simple Ansatz for Treating a Large Number of Chromophores. *J. Chem. Phys.* **2020**, *152* (20), 204113.

(12) Li, T. E.; Cui, B.; Subotnik, J. E.; Nitzan, A. Molecular Polaritonics: Chemical Dynamics Under Strong Light-Matter Coupling. *Annu. Rev. Phys. Chem.* **2022**, *73* (1), 43−71.

(13) Li, T. E.; Nitzan, A.; Subotnik, J. E. Polariton Relaxation under Vibrational Strong Coupling: Comparing Cavity Molecular Dynamics Simulations against Fermi's Golden Rule Rate. *J. Chem. Phys.* **2022**, *156* (13), 134106.

(14) Fowler-Wright, P.; Lovett, B. W.; Keeling, J. Efficient Many-Body Non-Markovian Dynamics of Organic Polaritons. *Phys. Rev. Lett.* **2022**, *129* (17), 173001.

(15) Strashko, A.; Kirton, P.; Keeling, J. Organic Polariton Lasing and the Weak to Strong Coupling Crossover. *Phys. Rev. Lett.* **2018**, *121* (19), 193601.

(16) Del Pino, J.; Schröder, F. A. Y. N.; Chin, A. W.; Feist, J.; Garcia-Vidal, F. J. Tensor Network Simulation of Non-Markovian Dynamics in Organic Polaritons. *Phys. Rev. Lett.* **2018**, *121* (22), 227401.

(17) Engelhardt, G.; Cao, J. Unusual Dynamical Properties of Disordered Polaritons in Microcavities. *Phys. Rev. B* **2022**, *105* (6), 064205.

(18) Wu, N.; Feist, J.; Garcia-Vidal, F. J. When Polarons Meet Polaritons: Exciton-Vibration Interactions in Organic Molecules Strongly Coupled to Confined Light Fields. *Phys. Rev. B* **2016**, *94* (19), 195409.

(19) Mandal, A.; Taylor, M. A. D.; Weight, B. M.; Koessler, E. R.; Li, X.; Huo, P. Theoretical Advances in Polariton Chemistry and Molecular Cavity Quantum Electrodynamics. *Chem. Rev.* **2023**, *123* (16), 9786−9879.

(20) Foley, J. J.; McTague, J. F.; DePrince, A. E. *Ab Initio* Methods for Polariton Chemistry. *Chem. Phys. Rev.* **2023**, *4* (4), 041301.
(21) Liebenthal, M. D.; Vu, N.; DePrince, A. E. Assessing the Effects of Orbital Relaxation and the Coherent-State Transformation in Quantum Electrodynamics Density Functional and Coupled-Cluster Theories. *J. Phys. Chem. A* **2023**, *127* (24), 5264−5275.
(22) Yang, J.; Ou, Q.; Pei, Z.; Wang, H.; Weng, B.; Shuai, Z.; Mullen, K.; Shao, Y. Quantum-Electrodynamical Time-Dependent Density Functional Theory within Gaussian Atomic Basis. *J. Chem. Phys.* **2021**, *155* (6), 064107.
(23) Mordovina, U.; Bungey, C.; Appel, H.; Knowles, P. J.; Rubio, A.; Manby, F. R. Polaritonic Coupled-Cluster Theory. *Phys. Rev. Res.* **2020**, *2* (2), 023262.
(24) Weight, B. M.; Tretiak, S.; Zhang, Y. Diffusion Quantum Monte Carlo Approach to the Polaritonic Ground State. *Phys. Rev. A* **2024**, *109* (3), 032804.
(25) Flick, J.; Narang, P. Cavity-Correlated Electron-Nuclear Dynamics from First Principles. *Phys. Rev. Lett.* **2018**, *121* (11), 113002.
(26) Feynman, R. P. Simulating Physics with Computers. *Int. J. Theor. Phys.* **1982**, *21*, 467.
(27) Weinstein, Y. S.; Pravia, M. A.; Fortunato, E. M.; Lloyd, S.; Cory, D. G. Implementation of the Quantum Fourier Transform. *Phys. Rev. Lett.* **2001**, *86* (9), 1889−1891.
(28) Mitchell, M. W.; Lundeen, J. S.; Steinberg, A. M. Super-Resolving Phase Measurements with a Multiphoton Entangled State. *Nature* **2004**, *429* (6988), 161−164.
(29) Shor, P. W. Polynomial-Time Algorithms for Prime Factorization and Discrete Logarithms on a Quantum Computer. *SIAM J. Comput.* **1997**, *26* (5), 1484−1509.
(30) Preskill, J. Quantum Computing in the NISQ Era and Beyond. *Quantum* **2018**, *2*, 79.
(31) Fedorov, D. A.; Peng, B.; Govind, N.; Alexeev, Y. VQE Method: A Short Survey and Recent Developments. *Mater. Theory* **2022**, *6* (1), 2.
(32) Peruzzo, A.; McClean, J.; Shadbolt, P.; Yung, M.-H.; Zhou, X.-Q.; Love, P. J.; Aspuru-Guzik, A.; O'Brien, J. L. A Variational Eigenvalue Solver on a Photonic Quantum Processor. *Nat. Commun.* **2014**, *5* (1), 4213.
(33) Bharti, K.; Cervera-Lierta, A.; Kyaw, T. H.; Haug, T.; Alperin-Lea, S.; Anand, A.; Degroote, M.; Heimonen, H.; Kottmann, J. S.; Menke, T.; Mok, W.-K.; Sim, S.; Kwek, L.-C.; Aspuru-Guzik, A. Noisy Intermediate-Scale Quantum Algorithms. *Rev. Mod. Phys.* **2022**, *94* (1), 015004.
(34) Cao, Y.; Romero, J.; Olson, J. P.; Degroote, M.; Johnson, P. D.; Kieferová, M.; Kivlichan, I. D.; Menke, T.; Peropadre, B.; Sawaya, N. P. D.; Sim, S.; Veis, L.; Aspuru-Guzik, A. Quantum Chemistry in the Age of Quantum Computing. *Chem. Rev.* **2019**, *119* (19), 10856−10915.
(35) Wecker, D.; Hastings, M. B.; Troyer, M. Progress towards Practical Quantum Variational Algorithms. *Phys. Rev. A* **2015**, *92* (4), 042303.
(36) Vaquero-Sabater, N.; Carreras, A.; Orús, R.; Mayhall, N. J.; Casanova, D. Physically Motivated Improvements of Variational Quantum Eigensolvers. *J. Chem. Theory Comput.* **2024**, *20*, 5133.
(37) Guo, S.; Sun, J.; Qian, H.; Gong, M.; Zhang, Y.; Chen, F.; Ye, Y.; Wu, Y.; Cao, S.; Liu, K.; Zha, C.; Ying, C.; Zhu, Q.; Huang, H.-L.; Zhao, Y.; Li, S.; Wang, S.; Yu, J.; Fan, D.; Wu, D.; Su, H.; Deng, H.; Rong, H.; Li, Y.; Zhang, K.; Chung, T.-H.; Liang, F.; Lin, J.; Xu, Y.; Sun, L.; Guo, C.; Li, N.; Huo, Y.-H.; Peng, C.-Z.; Lu, C.-Y.; Yuan, X.; Zhu, X.; Pan, J.-W. Experimental Quantum Computational Chemistry with Optimized Unitary Coupled Cluster Ansatz. *Nat. Phys.* **2024**, *20*, 1240.
(38) Hempel, C.; Maier, C.; Romero, J.; McClean, J.; Monz, T.; Shen, H.; Jurcevic, P.; Lanyon, B. P.; Love, P.; Babbush, R.; Aspuru-Guzik, A.; Blatt, R.; Roos, C. F. Quantum Chemistry Calculations on a Trapped-Ion Quantum Simulator. *Phys. Rev. X* **2018**, *8* (3), 031022.
(39) Lyu, C.; Montenegro, V.; Bayat, A. Accelerated Variational Algorithms for Digital Quantum Simulation of Many-Body Ground States. *Quantum* **2020**, *4*, 324.
(40) Araz, J. Y.; Spannowsky, M.; Wingate, M. Exploring Thermal Equilibria of the Fermi-Hubbard Model with Variational Quantum Algorithms. *Phys. Rev. A* **2024**, *109* (6), 062422.
(41) Yuan, X.; Endo, S.; Zhao, Q.; Li, Y.; Benjamin, S. Theory of Variational Quantum Simulation. *Quantum* **2019**, *3*, 191.
(42) Li, Y.; Benjamin, S. C. Efficient Variational Quantum Simulator Incorporating Active Error Minimization. *Phys. Rev. X* **2017**, *7* (2), 021050.
(43) Boy, C.; Wales, D. J. Energy Landscapes for the Quantum Approximate Optimization Algorithm. *Phys. Rev. A* **2024**, *109* (6), 062602.
(44) Chng, B. X. K.; Ying, W.; Lai, Y.; Vamivakas, A. N.; Cundiff, S. T.; Krauss, T. D.; Huo, P. Mechanism of Molecular Polariton Decoherence in the Collective Light-Matter Couplings Regime. *J. Phys. Chem. Lett.* **2024**, *15* (47), 11773−11783.
(45) Denning, E. V.; Bundgaard-Nielsen, M.; Mørk, J. Optical Signatures of Electron-Phonon Decoupling Due to Strong Light-Matter Interactions. *Phys. Rev. B* **2020**, *102* (23), 235303.
(46) Karanikolas, V.; Thanopulos, I.; Paspalakis, E. Strong Coupling Regime and Bound States in the Continuum between a Quantum Emitter and Phonon-Polariton Modes. *Opt. Express* **2021**, *29* (15), 23408−23420.
(47) Baydin, A.; Manjappa, M.; Mishra, S. S.; Xu, H.; Doumani, J.; Tay, F.; Kim, D.; Hernandez, F. G. G.; Rappl, P. H. O.; Abramof, E.; Singh, R.; Kono, J. Terahertz Cavity Phonon Polaritons in the Deep-Strong Coupling Regime. In *Proceedings of the 2023 48th International Conference on Infrared, Millimeter, and Terahertz Waves (IRMMW-THz)*, Montreal, Canada, September 17−22, 2023; IEEE, 2023.
(48) Barra-Burillo, M.; Muniain, U.; Catalano, S.; Autore, M.; Casanova, F.; Hueso, L. E.; Aizpurua, J.; Esteban, R.; Hillenbrand, R. Microcavity Phonon Polaritons from the Weak to the Ultrastrong Phonon-Photon Coupling Regime. *Nat. Commun.* **2021**, *12* (1), 6206.
(49) Tudorovskaya, M.; Muñoz Ramo, D. Quantum Computing Simulation of a Mixed Spin-Boson Hamiltonian and Its Performance for a Cavity Quantum Electrodynamics Problem. *Phys. Rev. A* **2024**, *109* (3), 032612.
(50) Dupont, M.; Didier, N.; Hodson, M. J.; Moore, J. E.; Reagor, M. J. Entanglement Perspective on the Quantum Approximate Optimization Algorithm. *Phys. Rev. A* **2022**, *106* (2), 022423.
(51) Miessen, A.; Ollitrault, P. J.; Tavernelli, I. Quantum algorithms for quantum dynamics: A performance study on the spin-boson model. *Phys. Rev. Res.* **2021**, *3*, 043212.
(52) Somma, R.; Ortiz, G.; Knill, E.; Gubernatis, J. Quantum Simulations of Physics Problems. *Int. J. Quantum Inf.* **2003**, *1* (3), 189−206.
(53) Jaderberg, B.; Eisfeld, A.; Jaksch, D.; Mostame, S. Recompilation-Enhanced Simulation of Electron-Phonon Dynamics on IBM Quantum Computers. *New J. Phys.* **2022**, *24* (9), 093017.
(54) Macridin, A.; Spentzouris, P.; Amundson, J.; Harnik, R. Electron-Phonon Systems on a Universal Quantum Computer. *Phys. Rev. Lett.* **2018**, *121* (11), 110504.
(55) Di Matteo, O.; McCoy, A.; Gysbers, P.; Miyagi, T.; Woloshyn, R. M.; Navrátil, P. Improving Hamiltonian encodings with the Gray code. *Phys. Rev. A* **2021**, *103*, 042405.
(56) Li, W.; Ren, J.; Huai, S.; Cai, T.; Shuai, Z.; Zhang, S. Efficient Quantum Simulation of Electron-Phonon Systems by Variational Basis State Encoder. *Phys. Rev. Res.* **2023**, *5* (2), 023046.
(57) Nielsen, M. A.; Chuang, I. L. *Quantum computation and quantum information*, 10th anniversary ed.; Cambridge University Press, 2010. https://www.cambridge.org/cn/universitypress/subjects/physics/quantum-physics-quantum-information-and-quantum-computation/quantum-computation-and-quantum-information-10th-anniversary-edition (accessed 2024-12-26).
(58) Shor, P. W. Scheme for Reducing Decoherence in Quantum Computer Memory. *Phys. Rev. A* **1995**, *52* (4), R2493−R2496.

(59) Fowler, A. G.; Mariantoni, M.; Martinis, J. M.; Cleland, A. N. Surface Codes: Towards Practical Large-Scale Quantum Computation. *Phys. Rev. A* **2012**, *86* (3), 032324.
(60) Brun, T. A. Quantum Error Correction. *Oxford Research Encyclopedia of Physics* **2020**, DOI: 10.1093/acrefore/9780190871994.013.35.
(61) Viola, L.; Knill, E.; Lloyd, S. Dynamical Decoupling of Open Quantum Systems. *Phys. Rev. Lett.* **1999**, *82* (12), 2417−2421.
(62) Google AI Quantum and Collaborators; et al. Hartree-Fock on a superconducting qubit quantum computer. *Science* **2020**, *369*, 1084−1089.
(63) McCaskey, A. J.; Parks, Z. P.; Jakowski, J.; Moore, S. V.; Morris, T. D.; Humble, T. S.; Pooser, R. C. Quantum chemistry as a benchmark for near-term quantum computers. *npj Quantum Inf.* **2019**, *5*, 99.
(64) Bravyi, S.; Sheldon, S.; Kandala, A.; Mckay, D. C.; Gambetta, J. M. Mitigating measurement errors in multiqubit experiments. *Phys. Rev. A* **2021**, *103*, 042605.
(65) Lolur, P.; Skogh, M.; Dobrautz, W.; Warren, C.; Biznarova, J.; Osman, A.; Tancredi, G.; Wendin, G.; Bylander, J.; Rahm, M. Reference-State Error Mitigation: A Strategy for High Accuracy Quantum Computation of Chemistry. *J. Chem. Theory Comput.* **2023**, *19* (3), 783−789.
(66) Sun, Q.; Berkelbach, T. C.; Blunt, N. S.; Booth, G. H.; Guo, S.; Li, Z.; Liu, J.; McClain, J. D.; Sayfutyarova, E. R.; Sharma, S.; Wouters, S.; Chan, G. K.-L. PySCF: The Python-Based Simulations of Chemistry Framework. *WIREs Comput. Mol. Sci.* **2018**, *8* (1), No. e1340.
(67) Weight, B.; Huo, P. Ab Initio Approaches to Simulate Molecular Polaritons: Properties and Quantum Dynamics | Theoretical and Computational Chemistry. *ChemRxiv* **2024**, xxx.
(68) Antoniou, P.; Suchanek, F.; Varner, J. F.; Foley, J. J. I. Role of Cavity Losses on Nonadiabatic Couplings and Dynamics in Polaritonic Chemistry. *J. Phys. Chem. Lett.* **2020**, *11* (21), 9063−9069.
(69) Nijjar, P.; Jankowska, J.; Prezhdo, O. V. Ehrenfest and Classical Path Dynamics with Decoherence and Detailed Balance. *J. Chem. Phys.* **2019**, *150* (20), 204124.
(70) Lyu, C.; Xu, X.; Yung, M.-H.; Bayat, A. Symmetry Enhanced Variational Quantum Spin Eigensolver. *Quantum* **2023**, *7*, 899.
(71) Li, W.; Allcock, J.; Cheng, L.; Zhang, S.-X.; Chen, Y.-Q.; Mailoa, J. P.; Shuai, Z.; Zhang, S. TenCirChem: An Efficient Quantum Computational Chemistry Package for the NISQ Era. *arXiv* **2023**, 2303.10825.
(72) Zhang, S.-X.; Allcock, J.; Wan, Z.-Q.; Liu, S.; Sun, J.; Yu, H.; Yang, X.-H.; Qiu, J.; Ye, Z.; Chen, Y.-Q.; Lee, C.-K.; Zheng, Y.-C.; Jian, S.-K.; Yao, H.; Hsieh, C.-Y.; Zhang, S. TensorCircuit: A Quantum Software Framework for the NISQ Era. *Quantum* **2023**, *7*, 912.
(73) Seeley, J. T.; Richard, M. J.; Love, P. J. The Bravyi-Kitaev Transformation for Quantum Computation of Electronic Structure. *J. Chem. Phys.* **2012**, *137* (22), 224109.
(74) Kandala, A.; Mezzacapo, A.; Temme, K.; Takita, M.; Brink, M.; Chow, J. M.; Gambetta, J. M. Hardware-Efficient Variational Quantum Eigensolver for Small Molecules and Quantum Magnets. *Nature* **2017**, *549* (7671), 242−246.